



ENHANCING THE BEAMFORMING MAP OF SPHERICAL ARRAYS AT LOW FREQUENCIES USING ACOUSTIC HOLOGRAPHY

Elisabet Tiana-Roig¹, Antoni Torras-Rosell², Efren Fernandez-Grande¹,
Cheol-Ho Jeong¹ and Finn T. Agerkvist¹

¹Acoustic Technology, Dep. Electrical Engineering, Technical University of Denmark
Ørsteds Plads 352, 2800 Kgs. Lyngby, Denmark

²DFM, Danish National Metrology Institute
Matematiktorvet 307, 2800 Kgs. Lyngby, Denmark

ABSTRACT

Recent studies have shown that the localization of acoustic sources based on circular arrays can be improved at low frequencies by combining beamforming with acoustic holography. This paper extends this technique to the three dimensional case by making use of spherical arrays. The pressure captured by a rigid spherical array under free-field conditions is used to compute the expected pressure on a virtual and larger sphere by means of acoustic holography. Beamforming is then applied with the pressure predicted at the virtual array. Since the virtual array has a larger radius compared to the one of the physical array, the low frequencies (the ones with larger wavelength) are better captured by the virtual array, and therefore, the performance of the resulting beamforming system is expected to improve at these frequencies. The proposed method is examined with simulations based on delay-and-sum beamforming. In addition, the principle is validated with experiments.

1 INTRODUCTION

Spherical arrays of microphones have been of interest in the last decade, because of the ability to measure in a three-dimensional sound field [1, 2]. Typically, these arrays are suitable for sound source localization using beamforming [3–6] and for sound recording in higher order reproduction systems such as Ambisonics [7–9].

Several strategies to improve the performance of beamforming systems have been suggested in the recent years. For example, it has been shown that arrays with flushed-mounted microphones on a rigid sphere perform better compared to open (or transparent) spherical arrays [2, 10, 11]. Besides this, different beamforming techniques have been designed for this geometry [6]. Among them, phase-mode (or spherical harmonics) beamforming is of particular interest, because it exploits the spherical geometry by decomposing the sound field in a series of spherical harmonics. Compared to the classical delay-and-sum beamforming, phase-mode beamforming presents a better directivity, at the expense of being more sensitive to noise [5]. In fact, delay-and-sum beamforming is a very robust technique, but it performs poorly at low frequencies, being omnidirectional in the worse case.

Inspired by an article on uniform circular arrays presented recently in Ref. [12], the present article examines the possibility of enhancing the localization of noise sources with spherical arrays at low frequencies by combining spherical acoustic holography [13–15] and delay-and-sum beamforming. The idea behind this concept is that for a given number of transducers, an array with a larger radius will perform better at low frequencies than a smaller array [2]. However, if one cannot change the geometry of the array, a simple solution to obtain a virtually larger array is illustrated in Fig. 1: the sound pressure is captured with a spherical array (rigid or transparent), and by means of acoustic holography the pressure is predicted at a virtual spherical array with larger radius. Finally the pressure at this virtual array is used for the beamforming process. The theory presented in this work is supplemented with simulations and measurements.

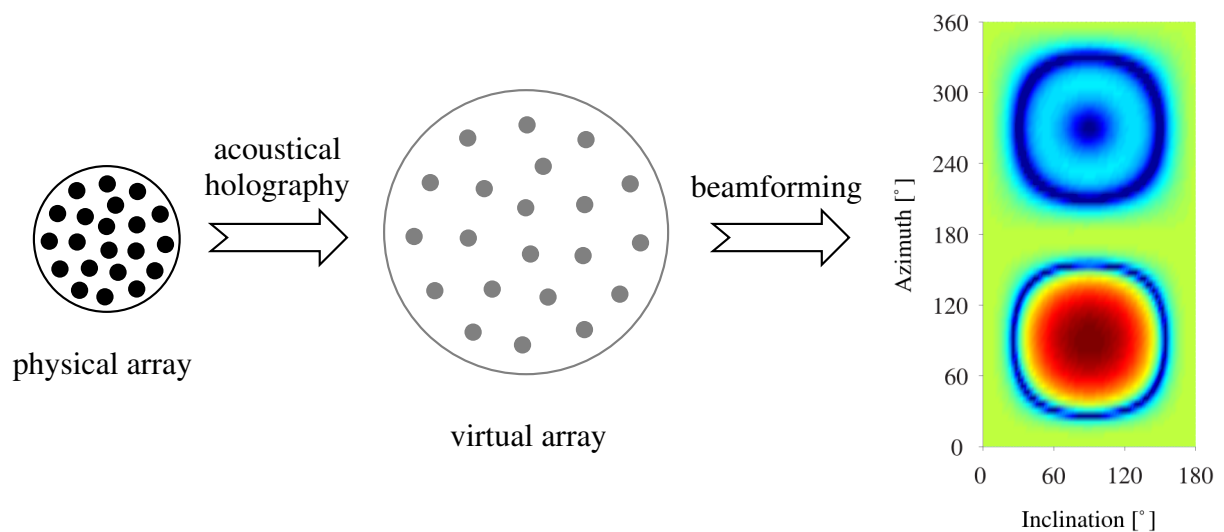


Figure 1: Procedure to obtain the beamforming map: the pressure captured by a spherical array is used to predict the pressure at a larger and virtual array with acoustic holography, and from this beamforming is carried out.

2 ACOUSTIC HOLOGRAPHY AND BEAMFORMING WITH A SPHERICAL ARRAY

2.1 Acoustic holography

Acoustic holography with a spherical array of transducers is a sound visualization technique that enables the reconstruction of a sound field over the three-dimensional space, based only on the sound pressure or particle velocity captured with the array. Acoustic holography measurements are usually performed very close to the source and the reconstruction lies somewhere between the measurement position and the source, as in near-field acoustic holography (NAH). However, in the present study, measurements in the far field of the sound source are of concern.

Let us consider a rigid spherical array with radius R centered at the origin of the coordinate system. The pressure at a point outside the array is given by the sum of the incident sound pressure and the scattered pressure due to the presence of the sphere,

$$p = p_{inc} + p_{sca}. \quad (1)$$

Given the spherical geometry, it makes sense to describe both pressures in terms of solutions of the Helmholtz equation in spherical coordinates (r, θ, φ) (θ being the inclination angle with respect to the z -axis and φ being the azimuth). The incident pressure, which is the one that would be measured if the scatterer was not present, must be described by means of spherical Bessel functions, because these are finite (even at the origin) [15, 16],

$$p_{inc}(kr, \theta, \varphi) = \sum_{n=0}^{\infty} \sum_{m=-n}^n A_{mn} j_n(kr) Y_n^m(\theta, \varphi), \quad (2)$$

where j_n is the spherical Bessel function of order n , and the terms Y_n^m are the so-called spherical harmonics,

$$Y_n^m(\theta, \varphi) = \sqrt{\frac{2n+1}{4\pi} \frac{(n-m)!}{(n+m)!}} P_n^m(\cos \theta) e^{jm\varphi}, \quad (3)$$

in which P_n^m is the associated Legendre function. Note that the time dependence $e^{-j\omega t}$ is omitted. The scattered pressure must be described as outgoing waves, represented in this case by the spherical Hankel functions of the first kind [17],

$$p_{sca}(kr, \theta, \varphi) = \sum_{n=0}^{\infty} \sum_{m=-n}^n B_{mn} h_n^{(1)}(kr) Y_n^m(\theta, \varphi), \quad (4)$$

where $h_n^{(1)}$ is the Hankel function of the first kind and order n .

The relationship between the coefficients A_{mn} and B_{mn} is given by the fact that the total radial velocity at the surface of the rigid sphere ($r = R$) is zero. From this condition it follows that

$$B_{mn} = -A_{mn} \frac{j_n'(kR)}{h_n^{(1)'}(kR)}, \quad (5)$$

where j'_n and $h_n^{(1)}$ are the radial derivatives of j_n and $h_n^{(1)}$. Therefore, the total pressure is

$$p(kr, \theta, \varphi) = \sum_{n=0}^{\infty} \sum_{m=-n}^n A_{mn} \left(j_n(kr) - \frac{j'_n(kR)}{h_n^{(1)}(kR)} h_n^{(1)}(kr) \right) Y_n^m(\theta, \varphi). \quad (6)$$

Since the pressure at the array is known, the coefficients A_{mn} can be retrieved by making use of the orthogonality relationship of the spherical harmonics,

$$\int_0^{2\pi} \int_0^{\pi} Y_n^m(\theta, \varphi) Y_v^\mu(\theta, \varphi)^* \sin \theta d\theta d\varphi = \delta_{nv} \delta_{m\mu}, \quad (7)$$

where δ_{nv} is the Kronecker delta function. Then, it can be shown that the coefficients A_{mn} are

$$A_{mn} = \frac{\int_0^{2\pi} \int_0^{\pi} p(kR, \theta, \varphi) Y_n^m(\theta, \varphi)^* \sin \theta d\theta d\varphi}{j_n(kR) - \frac{j'_n(kR)}{h_n^{(1)}(kR)} h_n^{(1)}(kR)}. \quad (8)$$

To implement this equation in practice, the integrals must be substituted by discrete summations, capable of fulfilling the discrete orthogonality relationship of the spherical harmonics, which has to be accounted for in the design of the array,

$$\sum_{i=0}^M \alpha_i Y_n^m(\theta_i, \varphi_i) Y_v^\mu(\theta_i, \varphi_i)^* = \delta_{nv} \delta_{m\mu} \quad \text{for} \quad v \leq N_{hol}, \quad n \leq N_{hol}, \quad (9)$$

where i represents the i th microphone at position (R, θ_i, φ_i) , M is the number of sensors, and α_i is an associated integration weight factor that guarantees orthogonality up to a certain order N_{hol} . Using the discrete orthogonality, the expression for the expansion coefficients A_{mn} results in [15]

$$A_{mn} = \frac{\sum_{i=1}^M \alpha_i p(kR, \theta_i, \varphi_i) Y_n^m(\theta_i, \varphi_i)^*}{j_n(kR) - \frac{j'_n(kR)}{h_n^{(1)}(kR)} h_n^{(1)}(kR)}. \quad (10)$$

This relationship assumes that the highest order of spherical harmonics included in the sound pressure is lower or equal to N_{hol} . This is a reasonable assumption as long as the value kR is about N_{hol} . When this requirement is not met aliasing occurs in the coefficients.

The coefficients A_{mn} can be used to compute the incident pressure and the scattered pressure separately (see Eqs. (2) and (4)) and the total pressure (see Eq. (6)) at a point (r, θ, φ) .

2.2 Beamforming

Beamforming is a signal processing technique well used for localization of sound sources. There are several beamforming methods, but in the present study, delay-and-sum beamforming is chosen. Although this method is the oldest one, it is still widely used due to its robustness. It consists of delaying the signals of each array microphone by a certain amount and adding them together, to reinforce the resulting signal. Depending on the delay applied to the different microphones, the array is steered to a particular direction, whereas other directions are totally or partially attenuated [18]. Since in the current study the array is mounted on a rigid sphere,

it is simpler to express the beamforming output in the spatial frequency domain, because this allows us to compensate for the effect of the scatterer. In this domain the output is

$$b(kR, \theta, \varphi) = B \sum_{i=1}^M w_i \tilde{p}(kR, \theta_i, \varphi_i) p(kR, \theta_i, \varphi_i | \theta, \varphi)^*, \quad (11)$$

where B is a scaling factor, w_i is a weighting factor, \tilde{p} is the measured pressure at the i th microphone, while p corresponds to the theoretical pressure at the i th microphone due to a source in the far-field at (θ, φ) . It can be shown that the pressure at (R, θ_i, φ_i) due to a plane wave created by a source at (θ, φ) is [4]

$$p(R, \theta_i, \varphi_i) = \sum_{n=0}^{\infty} \sum_{m=-n}^n Q_n(kR) Y_n^m(\theta_i, \varphi_i) Y_n^m(\theta, \varphi)^*, \quad (12)$$

where Q_n is

$$Q_n(kR) = 4\pi(-j)^n \left(j_n(kR) - \frac{j_n'(kR)}{h_n^{(1)'(kR)}} h_n^{(1)}(kR) \right). \quad (13)$$

Making use of this expression the output of the delay-and-sum beamformer is

$$b(kR, \theta, \varphi) = B \sum_{i=1}^M w_i \tilde{p}(kR, \theta_i, \varphi_i) \sum_{n=0}^N \left(Q_n(kR) \sum_{m=-n}^n Y_n^m(\theta_i, \varphi_i) Y_n^m(\theta, \varphi)^* \right)^*. \quad (14)$$

Note that the second summation has to be truncated at N for the real implementation. A reasonable value is $N \approx kR + 1$. By making use of the addition theorem [19] that states that

$$P_n(\cos \psi_q) = \frac{4\pi}{2n+1} \sum_{m=-n}^n Y_n^m(\theta, \varphi) Y_n^m(\theta_q, \varphi_q)^*, \quad (15)$$

where

$$\cos(\psi_q) = \cos \theta \cos \theta_q + \sin \theta \sin \theta_q \cos(\varphi - \varphi_q), \quad (16)$$

the beamformer output can be simplified:

$$b_N(kR, \theta, \varphi) = B \sum_{i=1}^M w_i p(kR, \theta_i, \varphi_i) \sum_{n=0}^N \frac{2n+1}{4\pi} Q_n(kR)^* P_n(\cos \psi_i). \quad (17)$$

To have an output equal to one when a plane wave with amplitude unity is measured at the array, it is easy to show that the value of B should be

$$B = \frac{1}{\sum_{i=0}^M w_i |p(kR, \theta_i, \varphi_i | \theta_0, \varphi_0)|^2}, \quad (18)$$

where θ_0 and φ_0 can be any angle, because with the spherical array the shape of the beampattern is independent of the steering direction, as it is practically shift-invariant [2].

2.3 Beamforming with a virtual array

As mentioned in the introduction, the goal of this study is to combine acoustic holography together with beamforming to improve the beamforming map at the low frequencies. To do this, the concept of virtual array has been presented; see Fig. 1. The pressure captured with a rigid spherical array is used to predict the pressure at a virtual spherical array with larger radius R_v , with virtual sensors placed at $(R_v, \theta_i, \varphi_i)$. The number of virtual sensors and their azimuth and inclination is kept the same as in the physical array. At this point we can consider two possibilities: 1) A virtual transparent array or 2) a virtual rigid array. For the virtual transparent array the expression is simply the incident pressure given in Eq. (2), evaluated at $r = R_v$. For the case of the virtual rigid array we should create a virtual spherical scatterer at R_v . To do that the incident pressure with coefficients A_{mn} (the ones obtained with the physical array) would impinge on the virtual sphere creating a virtual scattered pressure distributed at the surface of the virtual array. In accordance with Eqs. (4) and (5), the scattered pressure at the virtual transducers would be

$$p_{sca}(R_v, \theta_i, \varphi_i) = - \sum_{n=0}^{\infty} \sum_{m=-n}^n A_{mn} \frac{j'_n(kR_v)}{h_n^{(1)'}(kR_v)} h_n^{(1)}(kR_v) Y_n^m(\theta_i, \varphi_i). \quad (19)$$

Then, the total pressure at the virtual rigid array (at $r = R_v$) would be

$$p(R_v, \theta_i, \varphi_i) = \sum_{n=0}^{N_{hol}} \sum_{m=-n}^n A_{mn} \left(j_n(kR_v) - \frac{j'_n(kR_v)}{h_n^{(1)'}(kR_v)} h_n^{(1)}(kR_v) \right) Y_n^m(\theta_i, \varphi_i). \quad (20)$$

Since a rigid array has benefits compared to the transparent array, a virtual rigid spherical array is chosen for the current study.

To sum up, the procedure for combining holography and beamforming is the following one:

1. With a rigid spherical array measure the pressure at the microphones, $p(R, \theta_i, \varphi_i)$, where $i = 1, \dots, M$.
2. Insert $p(R, \theta_i, \varphi_i)$ into Eq. (10) to retrieve the coefficients A_{mn} to be used for acoustic holography.
3. Insert A_{mn} into Eq. (20) to obtain the predicted pressure at the virtual rigid array, $p(R_v, \theta_i, \varphi_i)$.
4. Use $p(R_v, \theta_i, \varphi_i)$ as input of the beamforming process, given in Eq. (17), but substituting R by R_v and using $N = kR_v + 1$. In the present study, the chosen weighting factor, w_i , equals the integration factor of the acoustic holography process, α_i .

3 SIMULATION STUDY

The focus of this section is to analyze the outcome of combining acoustic holography and beamforming by means of simulations. A rigid spherical array with radius $R = 9.75$ cm and 50 flush-mounted microphones has been assumed. The characteristics of the array used for the simulations are the same of that used for the measurements (which will be presented in Sec. 4).

A picture of the array can be seen in Fig. 2. The location of the microphones and their associated integration weights result from an optimization procedure inspired by Ref. [20]. This procedure guarantees that the discrete orthogonality relation across microphone positions given in Eq (9) is valid up to order $N_{hol} = 5$, if $kR \leq N_{hol}$. When this condition is not met, that is, above 2.8 kHz, aliasing occurs.



Figure 2: Prototype of spherical array used in the measurements.

The simulations assume a plane wave created at coordinates $(\theta, \varphi) = (90^\circ, 90^\circ)$. However, the origin of the plane wave is not important because the array is practically shift-invariant. The frequency range of analysis contains the low frequencies up to 2 kHz. To account for the background noise, a signal-to-noise ratio (SNR) of 30 dB at each microphone due to uniformly distributed noise is considered.

Following the procedure described in the previous section, acoustic holography is performed prior to beamforming, considering a virtual array with a radius 4 times larger than the radius of the physical array used to measure the actual sound field. The normalized beamformer output obtained with the physical array using conventional beamforming and the output of the virtual array are shown in Fig. 3 for a frequency of 210 Hz. For ease of reference, the ideal beamformer output that would be obtained in absence of noise with a physical array of the same radius is also shown.

As can be seen in the leftmost subfigure in Fig. 3, the output for the physical array is rather omnidirectional (the level is quite uniform). However the map is significantly improved when using the pressures at the virtual array as the source located at $(90^\circ, 90^\circ)$ is successfully identified. Moreover, the beamformer map resembles the map of the physical array of the same radius under ideal conditions to a high extent. The discrepancies are caused by the noise assumed for the virtual array simulation.

The performance is also quantified by two measures: the resolution and the maximum side lobe level (MSL). The resolution is the -3 dB width of the main lobe, whereas the MSL is the difference between the highest secondary lobe and the main lobe. For both measures, the smaller the values, the better. The resulting resolution for the azimuth and inclination angles, as well as the MSL, can be seen in Fig. 4, along the entire frequency range of interest. This figure includes the results with the physical array with radius R (black curve) and the ones obtained at four virtual arrays with radii $2R$ (continuous blue curve), $3R$ (continuous green curve), $4R$ (continuous red curve), and $5R$ (continuous cyan curve). The ideal curves obtained with arrays

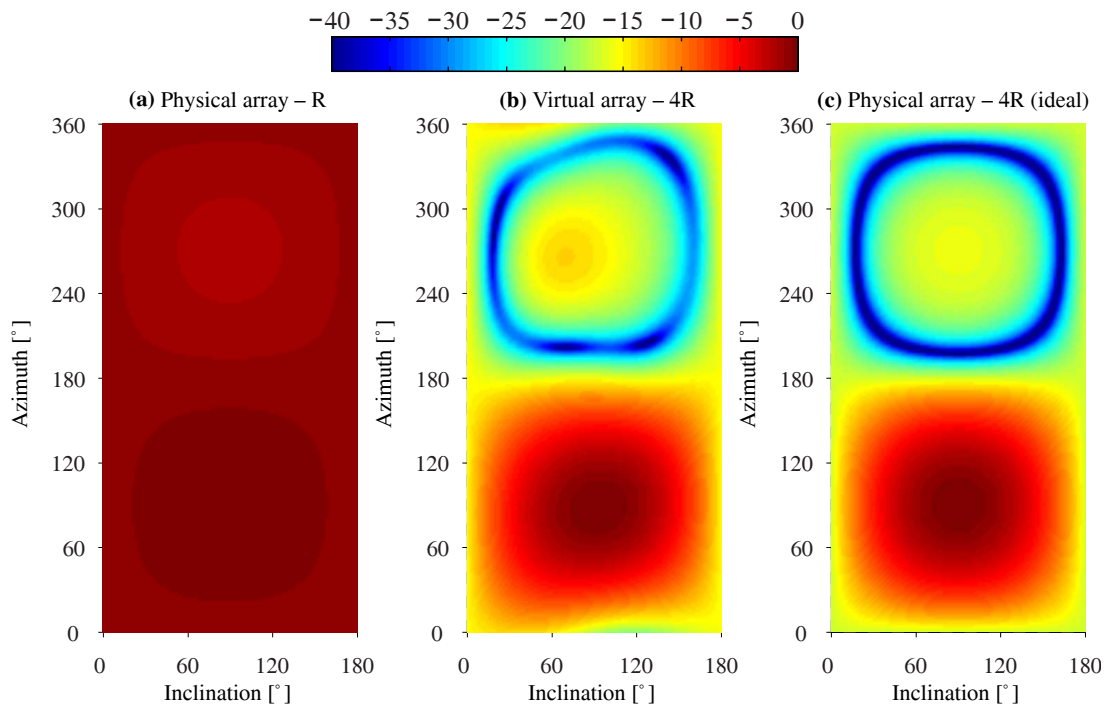


Figure 3: Normalized beamforming outputs at 210 Hz obtained with three rigid spherical arrays: one with radius $R = 9.75$ cm (left), a virtual array with radius $4R$ (middle) that results from the pressure at the physical array with radius R via acoustic holography, and an array of radius $4R$ with absence of noise (right). A SNR of 30 dB was assumed at each microphone of the physical array with radius R .

with radii $2R$ (dashed blue curve), $3R$ (dashed green curve), $4R$ (dashed red), and $5R$ (dashed cyan) for a SNR of infinity are also depicted.

In all cases it can be seen that both the resolution and the MSL are non-existent at low frequencies, meaning that the beamforming map is omnidirectional. From a particular frequency that depends on the array characteristics, the resolution improves, and sidelobes arise resulting in a certain MSL.

The resolution for both azimuth and inclination angles is improved towards the low frequencies with increasing radius of the virtual array, in comparison with the physical array of radius R used to capture the signals. Interestingly the curves of the virtual arrays are very similar to the ones of the arrays with the same radius under ideal conditions, although some deviations that become stronger with increasing virtual radius are observed for the virtual arrays of radii $3R$, $4R$ and $5R$.

On the other hand, the MSL of the virtual arrays is progressively shifted towards the low frequencies with increasing virtual radius. However, the MSL is more sensitive to noise than the resolution, as this measure worsens towards the high frequencies with increasing virtual radius, and the differences with the ideal MSL obtained with the physical arrays of the same radii in absence of noise (dashed curves) become larger. This is a consequence of the holography process itself, as the noise captured with the physical array is amplified with increasing distance to the reconstruction points, specifically for $r > R$. Therefore the reconstructed pressure deviates

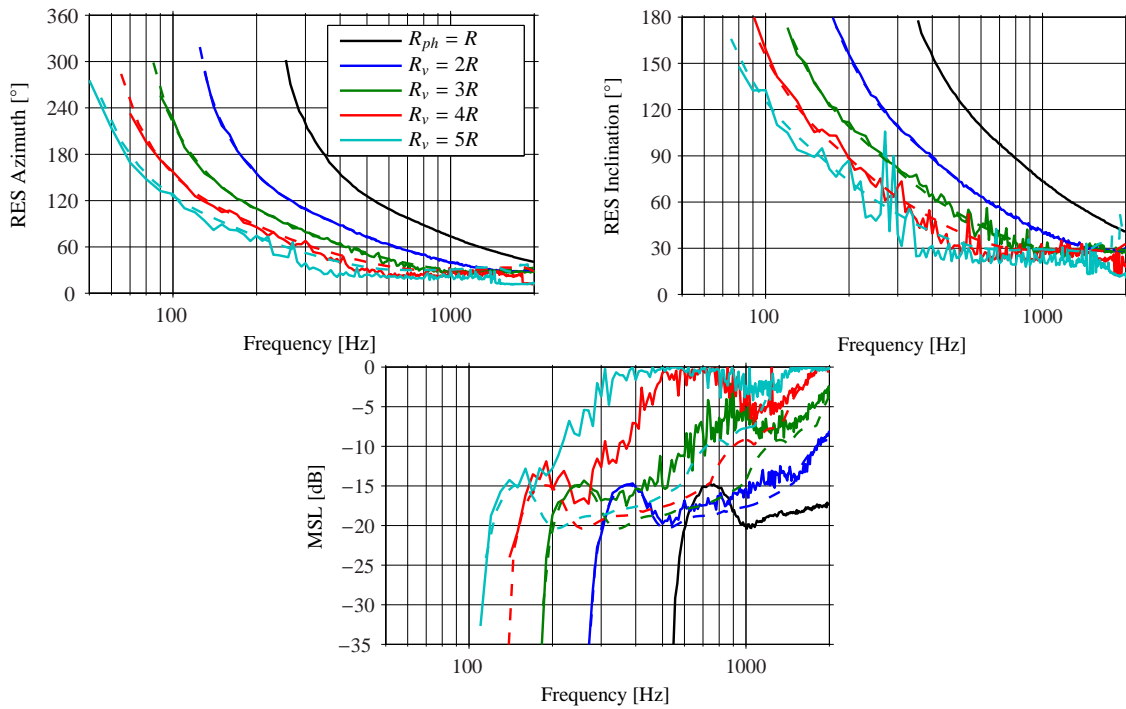


Figure 4: Resolution along the azimuth angle (top left), along the inclination angle (top right) and MSL (bottom) obtained by means of simulations with a physical array of radius $R = 9.75$ cm and 50 microphones (black continuous curve), as well as with four virtual arrays with radii $2R$, $3R$, $4R$ and $5R$ (blue, green, red and cyan continuous curves), that result from the pressure at the physical array with radius R via acoustic holography. The colored dashed lines show the results with arrays of the same radii as the virtual arrays, but with a SNR of infinity. A plane wave was created at $(\theta, \varphi) = (90^\circ, 90^\circ)$, and a SNR of 30 dB was assumed for the physical array with radius R .

from the ideal one [15], having a direct impact on the beamforming map, particularly on the sidelobes. Although not shown here, simulations reveal that the amplification of noise with an virtual array of radius $6R$ has dramatic influence on the beamforming map.

In conclusion, the results from the simulations show that one could take advantage of virtual arrays using the appropriate radius for each frequency, determined by the MSL. For example, in the case of study, a virtual array with radius $5R$ is suitable up to 170 Hz, from this frequency to about 280 Hz, one with radius $4R$ would be preferable, from 280 Hz to 400 Hz, $3R$ is more adequate, whereas from 400 Hz to 800 Hz a virtual array with radius $2R$ seems better. Above 800 Hz the physical array should be used as it is.

4 MEASUREMENT RESULTS

Measurements with a Brüel & Kjær (B&K) prototype array were carried out in a large anechoic chamber of about 1000 m^3 . The array, which can be seen in Fig. 2, had 50 1/4 in. microphones

B&K Type 4935 flush-mounted on a rigid sphere and 11 video cameras. Its radius, R , was 9.75 cm.

The set-up, shown in Fig. 5, consisted of a loudspeaker placed in the far field, at 5.8 m from the array. The loudspeaker height was 1 m and the array height 1.30 m. The array was placed such as the loudspeaker was detected at about $(\theta, \varphi) = (90^\circ, 90^\circ)$.

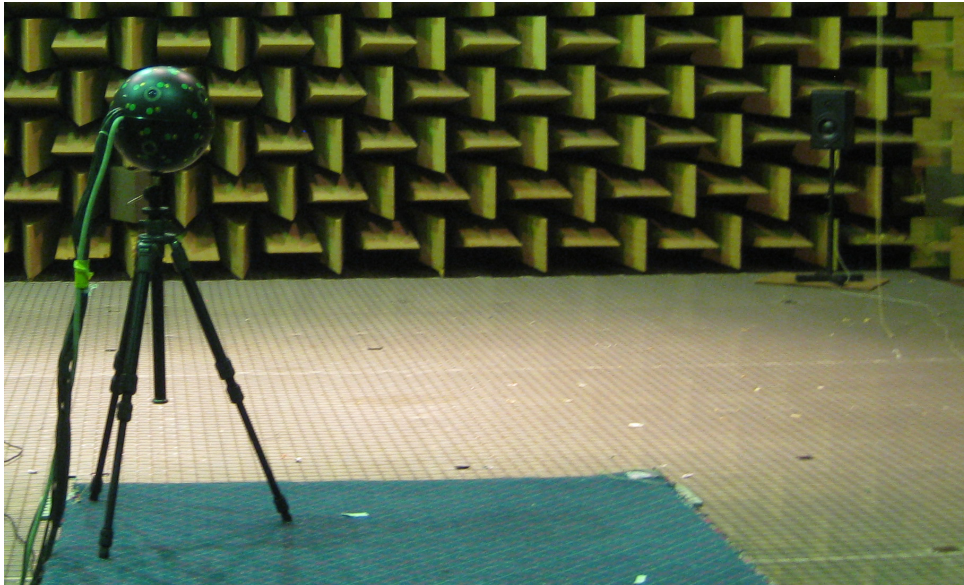


Figure 5: Measurement set-up.

The loudspeaker was fed with white noise. The signal level was adjusted so that the SNR at the array microphones was about 30 dB for most of the frequency range, although the SNR at the low frequencies was lower. The signal at each microphone was recorded with a B&K Pulse analyzer for 10 s. The data was segmented in blocks of 1 s using a Hanning window and a 50% overlapping. For each block, the crossspectra between each microphone and a reference, which was chosen to be microphone number one, was computed. The averaged crossspectra were used as input to conventional delay-and-sum beamforming. Besides, the data were used to predict the pressure at several virtual radii R_v , at $2R$, $3R$, $4R$ and $5R$, before applying beamforming, following the procedure indicated in Sec. 2.3. The resulting resolution for the azimuth and inclination angles, and the MSL with the physical and virtual arrays are shown in Fig. 6.

Both performance indicators follow the same trend observed in the simulations shown in Fig. 4: the resolution improves towards the low frequencies with increasing virtual radius, and the MSL is shifted towards the low frequencies, although its level increases with increasing virtual radius. The reader should keep in mind that the simulations were carried out assuming a SNR of 30 dB, which was not exactly the case for the measurements, especially after postprocessing the data, and therefore, some deviations between simulations and results are expected. In this regard, the MSL curves obtained with the virtual arrays are slightly better than the simulated ones.

These results confirm that the concept of virtual array can be used to enhance the performance of the beamforming system at low frequencies, with an appropriate virtual radius depending on the frequency. In this study, this makes it possible to extend the lower frequency of the physical

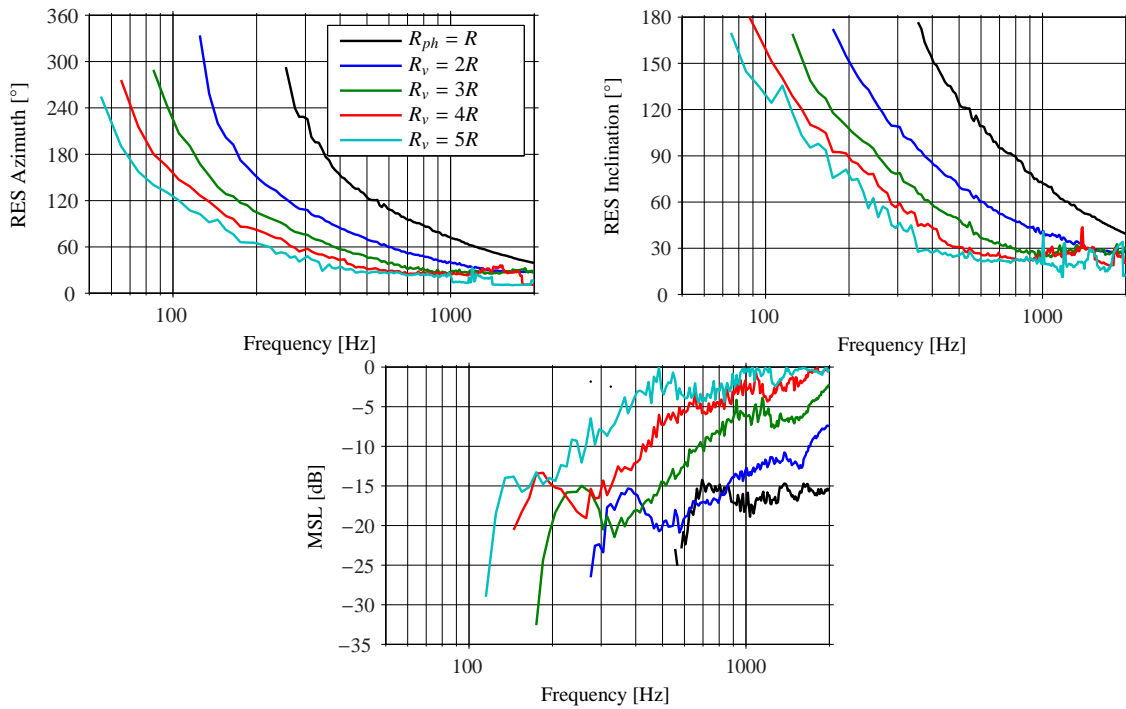


Figure 6: Resolution along the azimuth angle (top left), resolution along the inclination angle (top right) and MSL (bottom) obtained by means of measurements with a rigid spherical array of radius $R = 9.75$ cm and 50 microphones (black continuous curve), as well as the resulting resolution and MSL when considering four virtual spherical arrays with radii $2R$, $3R$, $4R$ and $5R$ (blue, green, red and cyan continuous curves), that result from the pressure at the physical array with radius R via acoustic holography. A plane wave was created at about $(\theta, \varphi) = (90^\circ, 90^\circ)$.

array down to about 55 Hz and 75 Hz in terms of resolution for the azimuth and the inclination angles, respectively, and 110 Hz in terms of MSL, in comparison with the original 250 Hz, 350 Hz and 550 Hz.

The advantage of combining acoustic holography and beamforming is further illustrated in Fig. 7, where the beamforming map obtained with the physical array at 210 Hz is shown, together with the maps obtained with virtual arrays with radii $2R$, $3R$ and $4R$. The larger the virtual radius, the clearer the map becomes, making it possible to localize better the sound source at its actual position, $(90^\circ, 90^\circ)$.

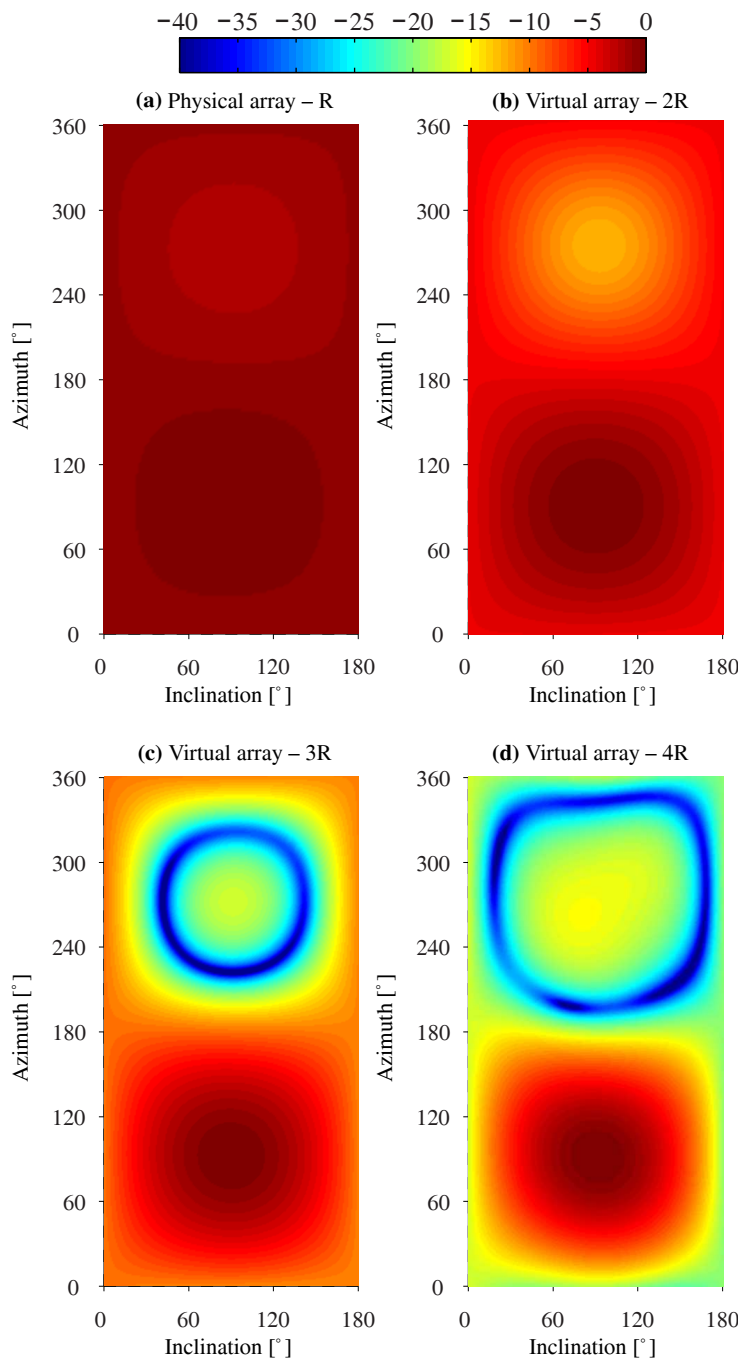


Figure 7: Normalized beamforming outputs at 210 Hz measured with a rigid spherical array with 50 microphones and radius $R = 9.75$ cm (top left), and three virtual rigid spherical arrays of radii $2R$ (top right), $3R$ (bottom left), and $4R$ (bottom middle), that result from the pressure at the physical array with radius R via acoustic holography.

5 CONCLUSIONS

Beamforming with spherical arrays is a powerful tool to localize and identify sound sources in a three-dimensional sound field. However, the resulting maps are difficult to interpret at low frequencies because such frequencies imply poor directivity, in particular with delay-and-sum beamforming. Inspired by the fact that the performance of the array would improve at low frequencies if a larger array was used, the present paper has presented a simple method that consists of predicting the pressure at a larger and virtual array by means of acoustic holography, and using it as input to the delay-and-sum beamforming procedure.

The performance of this combined approach has been assessed with two performance indicators, namely the resolution and the MSL. Both simulations and experimental results show that the resolution improves with increasing virtual radius, at the cost of the MSL, which is more sensitive to noise. This implies that the maximum virtual radius appropriate for each frequency is mainly determined by the MSL.

The use of holography prior to delay-and-sum beamforming offers new possibilities without any additional cost. At low frequencies the concept of virtual array can be used to improve the maps at such frequencies, while conventional beamforming can be applied directly at high frequencies.

ACKNOWLEDGMENTS

The authors would like to thank Karim Haddad, Brüel & Kjær, for lending us the spherical array used in the measurements.

REFERENCES

- [1] T. Abhayapala and Darren B. Ward. “Theory and design of high order sound field microphones using spherical microphone arrays.” *IEEE ICASSP*, II, 1949–1952, 2002.
- [2] J. Meyer and G. Elko. “A highly scalable spherical microphone array based on an orthonormal decomposition of the soundfield.” *IEEE ICASSP*, II, 1781–1784, 2002.
- [3] M. Park and B. Rafaely. “Sound-field analysis by plane-wave decomposition using spherical microphone array.” *J. Acoust. Soc. Am.*, 118(5), 3094–3103, 2005.
- [4] B. Rafaely. “Plane-wave decomposition of the sound field on a sphere by spherical convolution.” *J. Acoust. Soc. Am.*, 116 (4), 2149–2157, 2004.
- [5] B. Rafaely. “Phase-mode versus delay-and-sum spherical microphone array processing.” *IEEE Signal Processing Letters*, 12(10), 2005.
- [6] B. Rafaely. “Spatial sampling and beamforming for spherical microphone arrays.” *IEEE HSCMA*, 2008.
- [7] S. Favrot and M. Marschall. “Metrics for performance assessment of mixed-order ambisonics spherical microphone arrays.” *Proceedings of the AES 25th UK Conference*, 2012.

- [8] M. Marschall, S. Favrot, and J. Buchholz. “Robustness of a mixed-order Ambisonics microphone array for sound field reproduction.” *Proceedings of the AES 132nd Convention, Budapest, Hungary*, 2012.
- [9] S. Moreau, J. Daniel, and S. Bertet. “3D sound field recording with higher order Ambisonics - objective measurements and validation of a 4th order spherical microphone.” *Proceedings of the AES 120th Convention, Paris, France*, 2006.
- [10] B. Rafaely. “Analysis and design of spherical microphone arrays.” *IEEE Transactions on Speech and Audio Processing*, 13(1), 2005.
- [11] B. Rafaely and B. Weiss. “Spatial aliasing in spherical microphone arrays.” *IEEE Transactions on Signal Processing*, 55(3), 2007.
- [12] E. Tiana-Roig, A. Torras-Rosell, E. Fernandez-Grande, C.-H. Jeong, and F. Agerkvist. “Towards an enhanced performance of uniform circular arrays at low frequencies.” *Inter-noise 2013, Innsbruck, Austria*, 2013.
- [13] E.G. Williams, N. Valdivia, P.C. Herdic and J. Klos. “Volumetric acoustic vector intensity imager.” *J. Acoust. Soc. Am.*, 120(4), 1887–1897, 2006.
- [14] E.G. Williams and K. Takashima. “Vector intensity reconstructions in a volume surrounding a rigid spherical microphone array.” *J. Acoust. Soc. Am.*, 127(2), 773–783, 2010.
- [15] F. Jacobsen, G. Moreno-Pescador, E. Fernandez-Grande, and J. Hald. “Near field acoustic holography with microphones on a rigid sphere (L).” *J. Acoust. Soc. Am.*, 126(6), 3461–3464, 2011.
- [16] F. Jacobsen and P. Juhl. *Fundamentals of general linear acoustics*. Wiley, 2013.
- [17] F. Jacobsen, J. Hald, E. Fernandez-Grande, and G. Moreno. “Spherical near field acoustic holography with microphones on a rigid sphere.” *Acoustics’08, Paris*, 2008.
- [18] D. Johnson and D. Dudgeon. *Array Signal Processing Concepts and Techniques*. Prentice Hall, 1993.
- [19] G. Arfken and H. Weber. *Mathematical methods for physicists*. Elsevier Academic Press, Burlington, MA, 2005.
- [20] I. Sloan and R. Womersley. “External systems of points and numerical integration on the sphere.” *Advances in Computational Mathematics*, 21, 107–125, 2004.